



MODELING SOLIDIFICATION AND MUSHY ZONE DEFORMATION OF ALLOYS

E. M. S. Rizzo

Centro Federal de Educação Tecnológica do Espírito Santo
Coordenadoria de Metalurgia, C.P. 5139 – Vitória, ES, 29040-333, Brazil

R. G. Santos

Universidade Estadual de Campinas, Departamento de Engenharia de Materiais
Cx. P. 6122 – 13083-970 – Campinas, SP, Brazil

V. Raghavendra

C. Beckermann

Department of Mechanical Engineering, The University of Iowa,
Iowa City, IA 52242, USA.

Abstract: *The deformation of the partially solidified strand during near net shape continuous casting of thin slabs is only one example of a technologically important process where a mushy zone is mechanically altered in order to achieve improved grain structures and homogeneity. However, the phenomena occurring during plastic deformation of a solidifying mush are poorly understood, have not been observed directly, and have not been modeled in detail. A mathematical model that predicts the temperature and solid fraction profiles, liquid concentration evolution, and solid phase displacement during the deformation of a solidifying mush is presented. This model is derived considering a two-dimensional case, the volume averaging method, the enthalpy technique, and a coordinate transformation to avoid a changing mesh in a numerical solution. The numerical results are found to match the experimental behavior of metallic alloys during solidification with or without deformation.*

Key words: *near net shape, solidification, deformation, volume averaging, and modeling.*

1. INTRODUCTION

The manufacture of almost every man-made material involves the solidification process at some stage of the manufacturing process. Some of the important processes that involve solidification are foundry, welding, casting of ingots and continuous casting. Continuous casting is of such importance because it is a very economic method of forming a metallic component.

The composition variation within a solidified product is known as segregation. Segregation in an alloy is a result of solute rejection at the solidification front followed by its redistribution by diffusion and mass flow. Depending on the extension of composition variation, this defect is

classified as microsegregation, relative to grain scale, or macrosegregation, relative to the product scale. Macrosegregation affects the mechanical (ductility, strength, etc) and chemical properties (corrosion resistance) of materials in the product extension. It also affects precipitation of weak second phases, that was not expected if the initial composition was achieved, and porosity may be generated.

The formation of macrosegregation during metallic alloys' solidification is mainly caused by macroscopic movement of liquid metal and/or solid phases. Considering the case of continuous casting process, the following phenomena have been established as driving forces for this movement (Beckermann & Viskanta, 1993; Prescott & Incropera, 1994; Miyazawa & Schwerdtfeger, 1981):

- density changes due to phases transformations during the solidification and cooling;
- density changes due to temperature and compositional changes within a phase (natural convection);
- the action of gravitational field on a density gradient (buoyancy driven flows);
- drag forces from melt convection or from solid motion;
- external forces such as magnetic fields and forces applied on the surface (forced convection);
- solid stress due to solidification contraction or expansion (as a result of temperature variation or solid state phase transformation), metalostatic pressure, bulging between rolls and roll bending.

A review of the models previously employed to study the macrosegregation formation induced by deformation, particularly the centerline macrosegregation, demonstrates the range of approaches used by researchers (Moore, 1980; Lait & Brimacombe, 1982; Irvwing, 1993, Miyazawa & Schwerdtfeger, 1981; Lesoult & Sella, 1990; El-Bealy & Fredriksson, 1991). These approaches can be evaluated by considering the physical principles and the simplifying assumptions used to derive the correspondent equations that the authors assumed to explain the phenomenon of centerline macrosegregation.

Recently it has been proposed that the deformation of the partially solidified strand during near net shape continuous casting of thin slabs could reduce the defect of centerline macrosegregation. However, to the author's best knowledge, no mathematical model or even sets of complete experimental results that could be used to relate the process parameters and the macrosegregation reduction have been presented, i.e., when and how to apply the deformation. Examples of process parameters are the amount of deformation, the deformation rate, solid fraction and temperature at the moment of deformation and the effects of alloy composition.

2 – MODEL DESCRIPTION

The model development starts with a microscopic description. Conservation laws are introduced at the microscopic scale (Figure 1). Assumptions are made about the microscopic behavior of phases and interfaces, and accordingly, constitutive equations are also introduced at the microscopic scale (e.g. Newtonian fluid, Fickian diffusion, etc.). Resulting field equations are then averaged to obtain macroscopic field equations. Often in order to make the averaging procedure tractable and to obtain desirable results, many assumptions are made in the averaging process. These assumptions are typically related to the spatial and/or temporal distribution of properties, expected or magnitude of various terms, and existence of certain relations among various properties.

The main advantages of the averaging approach are that the available information at the microscale is passed on to the macroscale; the interfaces and their thermodynamic properties are explicitly taken into account; and the microstructure is more appropriately modeled. The disadvantage of this approach is that the types of restrictions imposed, especially those justifying neglect of various microscopic and macroscopic terms, may seriously limit the generality of the results and the opportunity to systematically explore fundamental behavior of complex phenomena. Also, construction of a full thermodynamic theory at the macroscale becomes intractable.

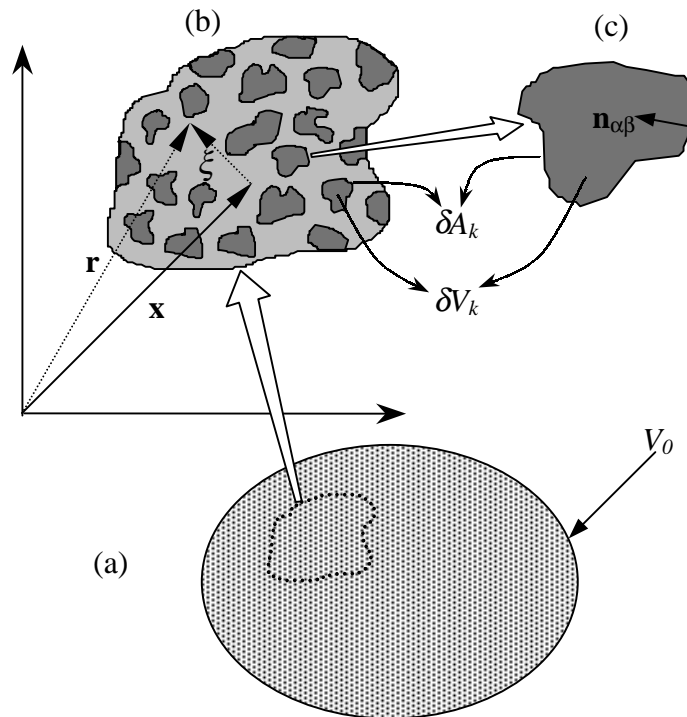


Figure 2 – (a) system or macroscopic level (continuum); (b) representative elementary volume on a microscopic level; (c) continuum solid at microscopic level.

Figure 1 presents the sketch for representing, at the grain scale (macroscopic level), the liquid and solid phases in the mushy region. The mushy zone comprises two interpenetrating phases (Wang & Beckermann, 1993). A porous medium is defined as a portion of space that is consisted of a solid phase and a void space. The interconnected voids are occupied by one or more fluid phases, which can flow through by the material.

On the void scale (microscopic scale) the flow quantities (velocity, pressure, etc.) will clearly be irregular (Nield & Bejan, 1992). However, in typical experiments, the quantities of interest are measured over areas that cross many voids, and such space-averaged (macroscopic scale) quantities change in a regular manner with respect to space and time, and hence are amenable to theoretical treatment.

Consider the transport of a general scalar specific quantity Ψ_k associate with a phase k in a multiphase mixture. For an arbitrary fixed control volume V of surface A , which is larger than a phase element but smaller than the characteristic domain dimension, conservation of Ψ_k can be expressed, in differential form for each phase (Ni, J.; Feller, J.; Beckermann, C., 1991; Bennon &

Incropera, 1987; Voller & Brent, 1989), as a balance of accumulation, net outflow by advection and diffusion, and volumetric production in a general form as follows:

$$\phi_k \rho_k \frac{\partial \langle \Psi_k \rangle^k}{\partial t} + \phi_k \rho_k \langle \mathbf{v}_k \rangle^k \cdot \nabla \langle \Psi_k \rangle^k = \nabla \cdot (\Lambda_k \nabla \langle \Psi_k \rangle^k) + S \quad (1)$$

or

$$\begin{aligned} & \frac{\partial (\phi_k \rho_k \langle \Psi_k \rangle^k)}{\partial t} + \nabla \cdot (\phi_k \rho_k \langle \mathbf{v}_k \rangle^k \langle \Psi_k \rangle^k - \Lambda_k \nabla \langle \Psi_k \rangle^k) = \\ & \langle \Psi_k \rangle^k \left[\frac{\partial (\phi_k \rho_k)}{\partial t} + \nabla \cdot (\phi_k \rho_k \langle \mathbf{v}_k \rangle^k) \right] + S \end{aligned} \quad (2)$$

where t = time, ϕ_k = solid fraction of a given phase k , ρ_k = density of a given phase k ; Λ_k = diffusion coefficient of a given phase k , S_k = volumetric source term which includes production or annihilation of Ψ_k .

In order to consider the grid changing due to deformation application (Figure 2), it is necessary to apply a coordinate transformation to the equation 1. If we consider a transformed, structured and orthogonal form (Maliska, 1995; Shyy *et al.*, 1996), the general equation in coordinates can be written as follows:

$$\begin{aligned} & \frac{\partial}{\partial \tau} \left(\frac{\phi_k \rho_k \langle \Psi_k \rangle^k}{J} \right) + \frac{\partial}{\partial \xi} \left[\begin{aligned} & \phi_k \rho_k \langle U'_k \rangle^k \langle \Psi_k \rangle^k - (\Lambda_k) J \alpha_{11} \frac{\partial \langle \Psi_k \rangle^k}{\partial \xi} \\ & - (\Lambda_k) J \alpha_{12} \frac{\partial \langle \Psi_k \rangle^k}{\partial \eta} \end{aligned} \right] + \\ & \frac{\partial}{\partial \eta} \left[\begin{aligned} & \phi_k \rho_k \langle V'_k \rangle^k \langle \Psi_k \rangle^k - (\Lambda_k) J \alpha_{21} \frac{\partial \langle \Psi_k \rangle^k}{\partial \eta} - (\Lambda_k) J \alpha_{22} \frac{\partial \langle \Psi_k \rangle^k}{\partial \xi} \end{aligned} \right] \\ & = \langle \Psi_k \rangle^k \left\{ \frac{\partial}{\partial \tau} \left(\frac{\phi_k \rho_k}{J} \right) + \frac{\partial}{\partial \xi} \left[\phi_k \rho_k \langle U'_k \rangle^k \right] + \frac{\partial}{\partial \eta} \left[\phi_k \rho_k \langle V'_k \rangle^k \right] \right\} + \hat{S} \end{aligned} \quad (3)$$

The metric tensor components α_{ij} (Shyy *et al.*, 1996; Maliska, 1995) and the Jacobian of the transformation, are given by

$$\alpha_{11} = \frac{a}{J^2} \quad (4) \quad \alpha_{12} = \alpha_{21} = \frac{d}{J^2} \quad (5) \quad \alpha_{22} = \frac{b}{J^2} \quad (6)$$

$$J = \det \begin{bmatrix} \xi_x & \xi_y \\ \eta_x & \eta_y \end{bmatrix} = \det \begin{bmatrix} x_\xi & x_\eta \\ y_\xi & y_\eta \end{bmatrix}^{-1} \quad (7)$$

where:

$$a = \xi_x^2 + \xi_y^2 + \xi_z^2 \quad (8)$$

$$b = \eta_x^2 + \eta_y^2 + \eta_z^2 \quad (9)$$

$$d = \xi_x \eta_x + \xi_y \eta_y + \xi_z \eta_z \quad (10)$$

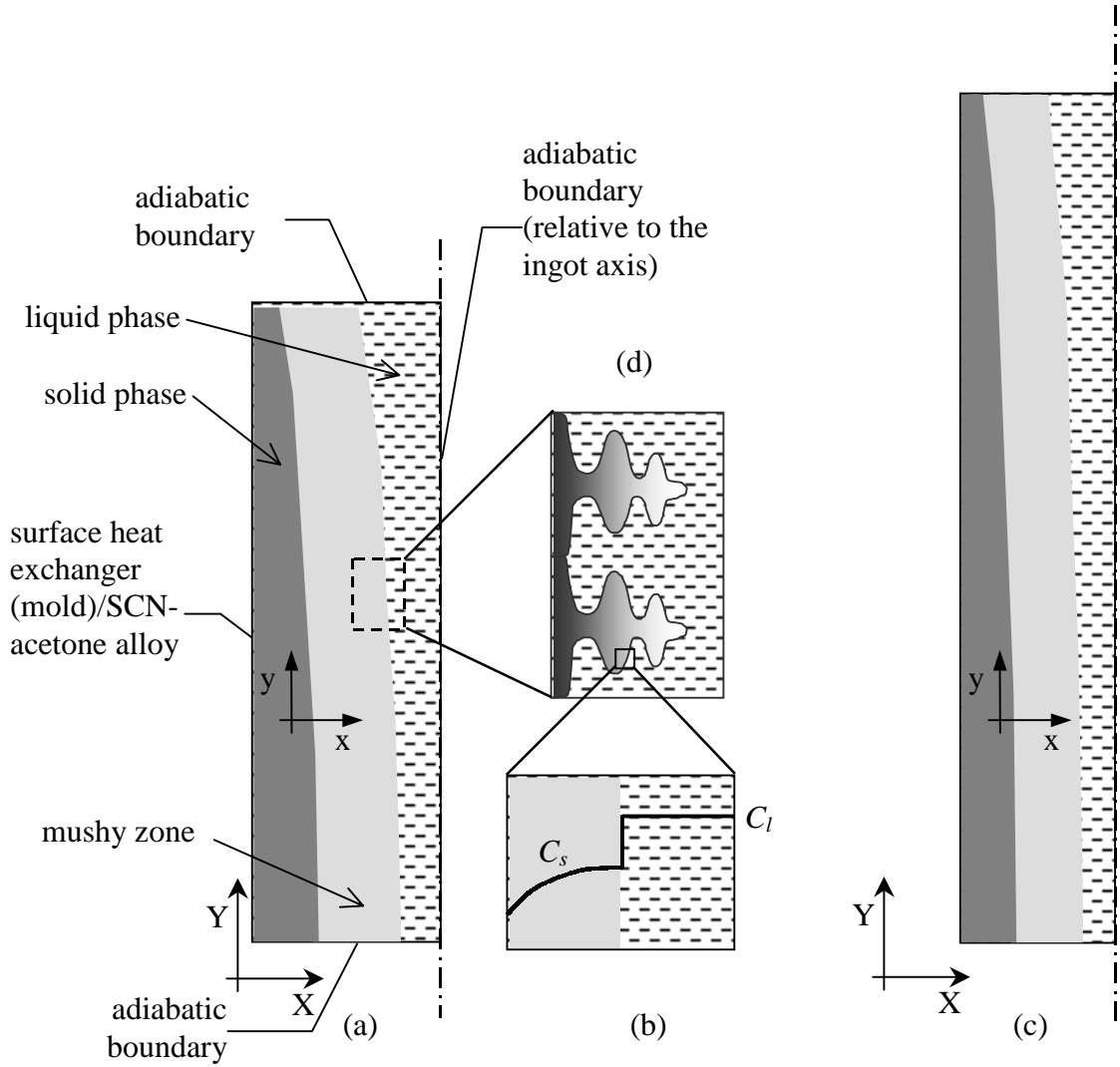


Figure 2 – (a) schematic illustration of the domain used in solidification simulations on a macroscopic scale prior to the deformation stage and (c) after the deformation stage; (b) a typical representative elementary volume; (d) a 1-D platelike model of a dendrite arm and illustration of a solid and liquid concentration profiles on a microscopic scale. The coordinate system X, Y is fixed and the coordinate system x, y moves with the solid phase translation, i.e., with the domain movement.

The metrics of transformation are defined as

$$\xi_x = J(y_\eta z_\gamma - y_\gamma z_\eta) \quad (11)$$

$$\xi_y = -J(x_\eta z_\gamma - x_\gamma z_\eta) \quad (12)$$

$$\eta_x = -J(y_\xi z_\gamma - y_\gamma z_\xi) \quad (13)$$

$$\eta_y = J(x_\xi z_\gamma - x_\gamma z_\xi) \quad (14)$$

$$x_\xi = \frac{1}{J}(\eta_y \gamma_z - \gamma_y \eta_z) \quad (15)$$

$$x_\eta = -\frac{1}{J}(\xi_y \gamma_z - \xi_z \gamma_y) \quad (16)$$

$$y_\xi = -\frac{1}{J}(\eta_x \gamma_z - \eta_z \gamma_x) \quad (17)$$

$$y_\eta = \frac{1}{J}(\xi_x \gamma_z - \gamma_x \xi_z) \quad (18)$$

$$\xi_t = \frac{\partial \xi}{\partial t} = -\xi_x x_\tau - \xi_y y_\tau \quad (19)$$

$$\eta_t = \frac{\partial \eta}{\partial t} = -\eta_x x_\tau - \eta_y y_\tau \quad (20)$$

The contravariant components of velocity vector, $\langle U_i' \rangle^l$ e $\langle V_i' \rangle^l$, are defined as follows (Shyy *et al*, 1996; Maliska, 1995, Zeng & Faghri, 1994):

$$\langle U_k' \rangle^k = \langle U_k \rangle^k - \langle U_k \rangle_M^k \quad (21)$$

$$\langle V_k' \rangle^k = \langle V_k \rangle^k - \langle V_k \rangle_M^k \quad (22)$$

Equation 3 can be rewritten as

$$\begin{aligned} & \frac{\partial}{\partial \tau} \left(\frac{\phi_k \rho_k \langle \Psi_k \rangle^k}{J} \right) + \frac{\partial}{\partial \xi} \left[\phi_k \rho_k \left(\langle u_k \rangle^k y_\eta - \langle v_k \rangle^k x_\eta - y_\eta x_\tau + x_\eta y_\tau \right) \langle \Psi_k \rangle^k \right] + \\ & \left[-(\Lambda_k) J \alpha_{11} \frac{\partial \langle \Psi_k \rangle^k}{\partial \xi} - (\Lambda_k) J \alpha_{12} \frac{\partial \langle \Psi_k \rangle^k}{\partial \eta} \right] + \\ & \frac{\partial}{\partial \eta} \left[\phi_k \rho_k \left(\langle v_k \rangle^k x_\xi - \langle u_k \rangle^k y_\xi - x_\xi y_\tau + y_\xi x_\tau \right) \langle \Psi_k \rangle^k - (\Lambda_k) J \alpha_{21} \frac{\partial \langle \Psi_k \rangle^k}{\partial \xi} - (\Lambda_k) J \alpha_{22} \frac{\partial \langle \Psi_k \rangle^k}{\partial \eta} \right] \\ & = \langle \Psi_k \rangle^k \left\{ \begin{aligned} & \frac{\partial}{\partial \tau} \left(\frac{\phi_k \rho_k}{J} \right) + \frac{\partial}{\partial \xi} \left[\phi_k \rho_k \left(\langle u_k \rangle^k y_\eta - \langle v_k \rangle^k x_\eta - y_\eta x_\tau + x_\eta y_\tau \right) \right] + \\ & \left[\frac{\partial}{\partial \eta} \left[\phi_k \rho_k \left(\langle v_k \rangle^k x_\xi - \langle u_k \rangle^k y_\xi - x_\xi y_\tau + y_\xi x_\tau \right) \right] \right] \end{aligned} \right\} + \widehat{S} \end{aligned} \quad (23)$$

The grid velocity is also a very important variable when we consider a coordinate transformation. In our case, the coordinate system of the solid phase relative to the moveable wall (x, y) is fixed at position $(0, y)$. Hence, the grid velocity is equal to zero at this position and it increases in the direction of $x = Sc$. The Cartesian components of the grid velocity vector (x_τ and y_τ) are calculated, for a given position i at a given time l , by

$$(x_\tau)_i^l = \frac{(x)_i^l - (x)_i^{l-1}}{\Delta t} \quad (24)$$

$$(y_\tau)_j^l = \frac{(y)_j^l - (y)_j^{l-1}}{\Delta t} \quad (25)$$

The grid velocity also varies according to the grid deformation pattern assumed for a given situation.

3 – NUMERICAL IMPLEMENTATION

For the results presented in this paper, an implicit, control-volume-based finite difference scheme has been used to discretize the conservation equations, and a power-law scheme has been used to evaluate the finite-difference coefficients. The velocity-pressure coupling in the momentum equations was handled using the SIMPLER algorithm (Patankar, 1980). A uniform grid deformation for the mesh is assumed during the deformation stage.

4 - RESULTS AND DISCUSSION

The model was applied to a case of deformation of an organic alloy (SCN-acetone). Succinonitrile (SCN) is a transparent organic substance in the liquid state that is used as an analogue material to study some phenomena related to the solidification processes. This material solidifies in a dendritic morphology. Experimental works with this alloy are been performing to compare the numerical results. Acetone was added to obtain an alloy behavior, i.e., to get a segregated profile during solidification. The initial composition for the experiments presented in this study is 11.3 wt% of acetone. The shape of the domain is rectangular and the initial and final sizes are 50 x 170 mm and 40 x 210 mm respectively. The boundary condition at the interface heat exchanger/SCN-acetone is the temperatures measured by thermocouples placed on this interface. The other boundaries are considered as adiabatic (Figure 2).

Space limitations prohibit the presentation of variables evolution plots for many times or during the deformation stage. Only two times were select to present the variables evolution. The first plot set (Figure 3) shows the variables at the time relative to the deformation beginning, i.e., at 26246 s from cooling start. The second plot set (Figure 4) is relative to the end of deformation end (26301 s). Figure 3 shows the (a) mesh, (b) temperature field, (c) solid fraction contours, (d) mixture concentration, (e) velocity field and liquid concentration contours and (f) a detail the velocity field for the time just before deformation was applied. Figure 4 shows the same results group for a time just after deformation.

Since the liquid is cooled as it falls along the left wall, the mushy zone is thicker near the bottom of the casting (Figure 3c) as well as the temperature drop is higher (Figure 3b). Figure 3e shows the convection pattern (buoyancy driven flow) in the bulk melt and in the mush zone typical of metallic alloys solidification. The liquid concentration contours in Figure 3e and solid fraction in Figure 3c show that the counterclockwise flow in the melt and the downward flow trough the mush zone carry some of this enriched liquid into the bulk melt.

Figure 4e and 4f show the changes in the liquid flow when a deformation is applied. The liquid is pushed upward carrying the solute enriched liquid from the regions near the center. It will promote a reduction in the acetone concentration in this region after a complete solidification. This implies in a tendency to reduce the centerline macrosegregation defect.

5 – CONCLUSIONS

The mathematical model and the numerical code presented can be useful to determine the suitable process parameters in order to reduce the macrosegregation defect in the continuous casting process. The numerical result patterns agree with experimental and other numerical codes results for the stage without deformation and with experimental observations when a domain deformation is applied. These preliminary simulations are now being compared to laboratory experiments with organic and metallic alloys.

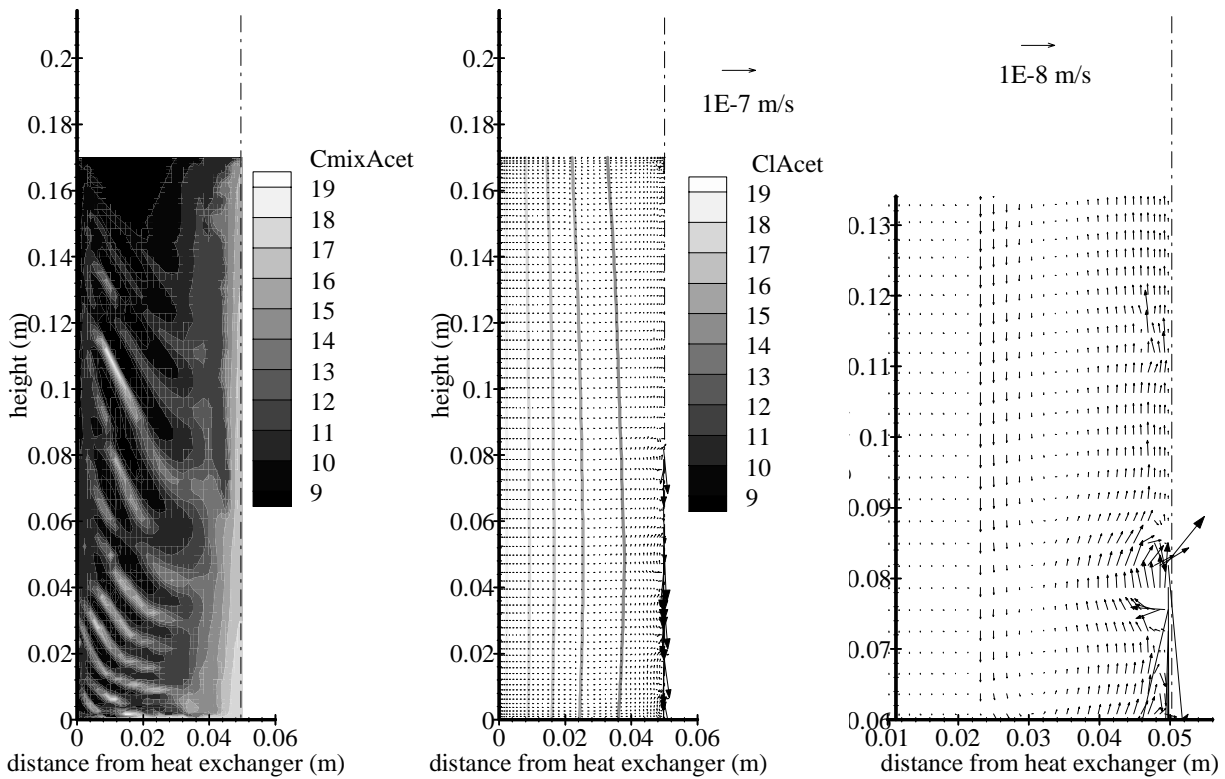
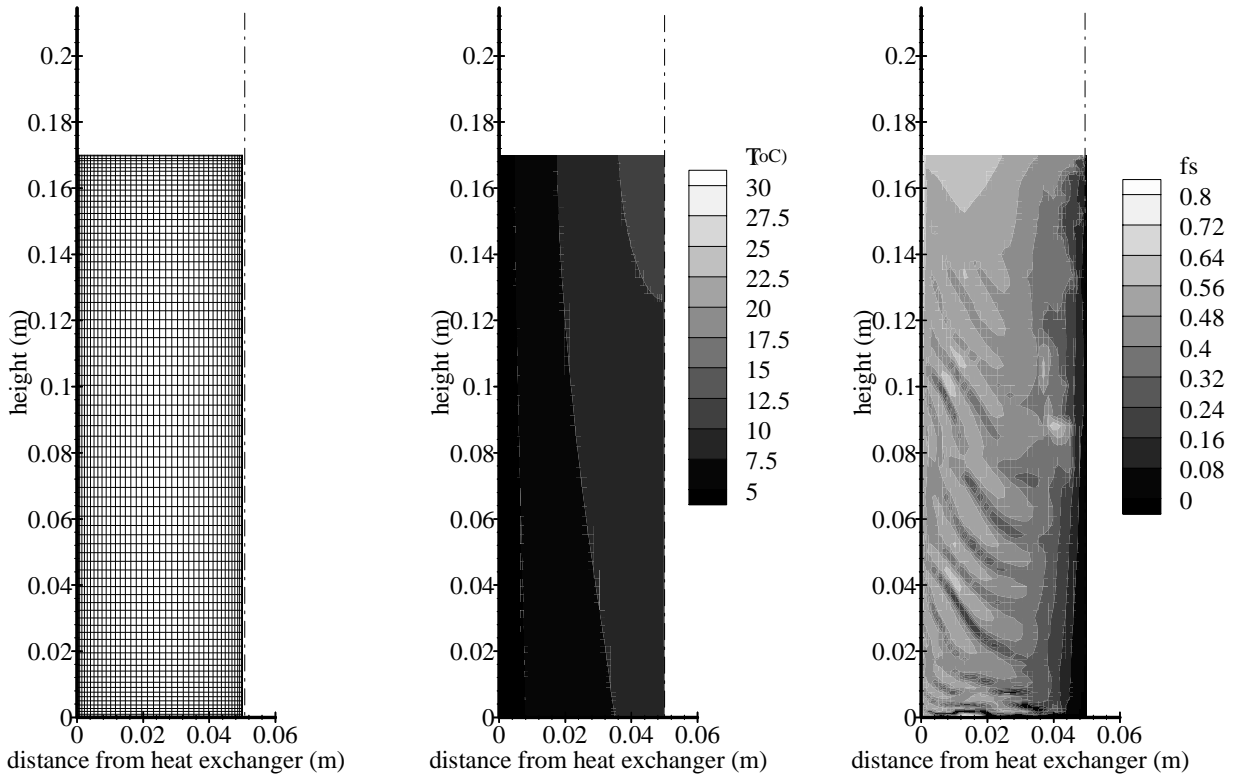


Figure 3 – (a) Mesh, (b) temperature field, (c) solid fraction contours, (d) mixture concentration, (e) velocity field and liquid concentration contours, (f) zoom for the velocity field. Initial concentration for acetone = 11.3 wt%; time = 20246 s, no deformation was applied.

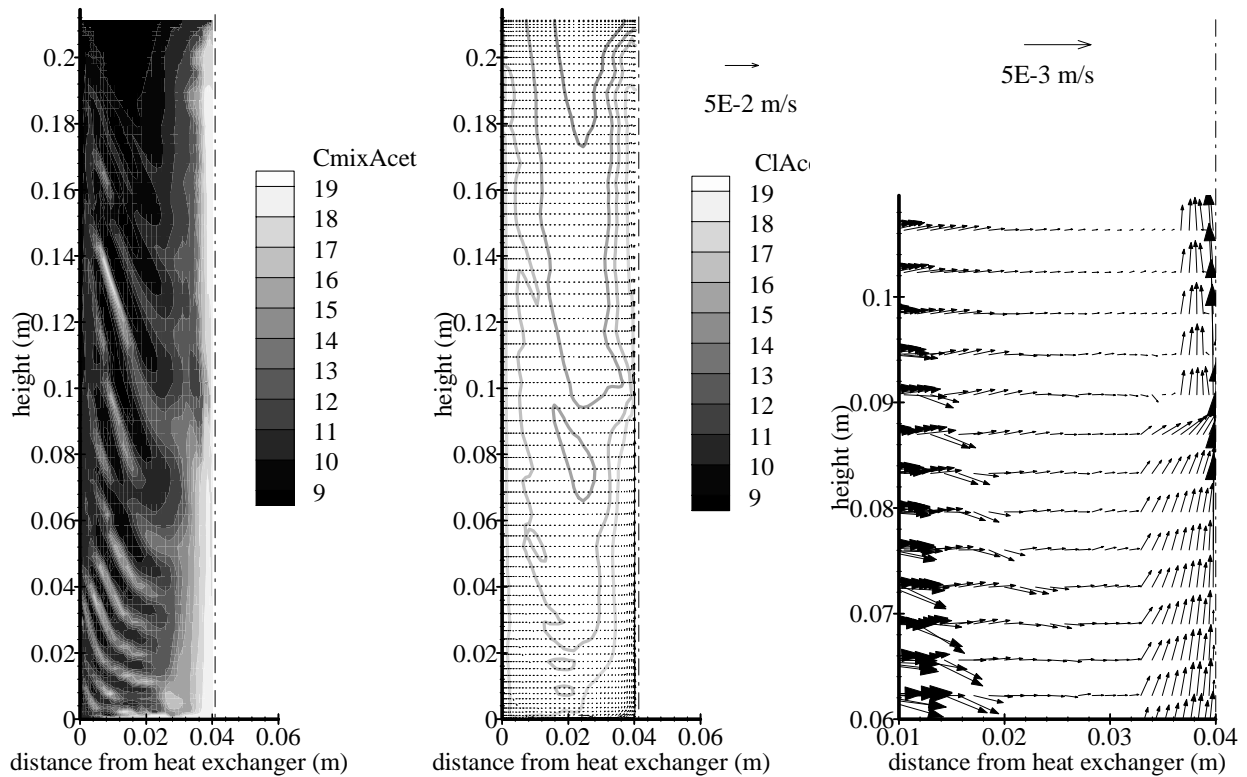
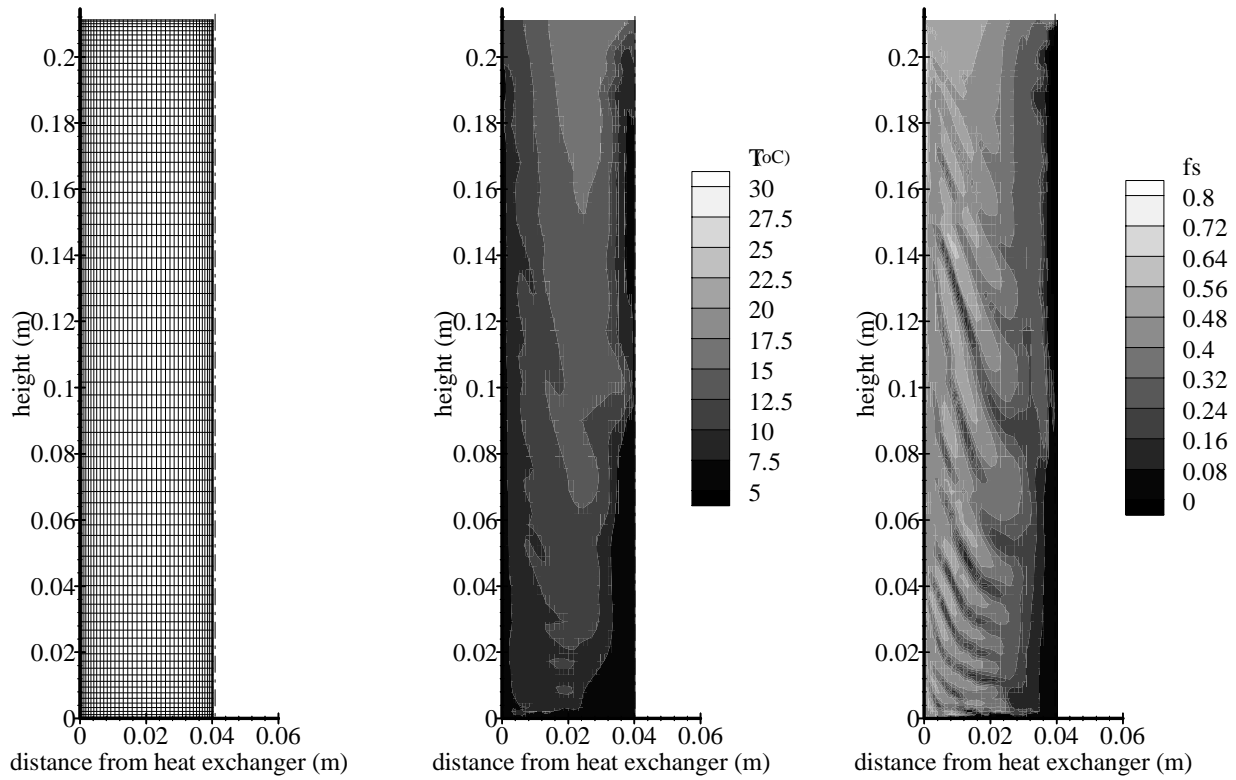


Figure 4 – (a) Mesh, (b) temperature field, (c) solid fraction contours, (d) mixture concentration, (e) velocity field and liquid concentration contours, (f) zoom for the velocity field. Initial concentration for acetone = 11.3 wt%; time = 20301 s, deformation was applied.

Acknowledgments

This work was supported by FAPESP (grant number 1997/2036-9) and Finep (Recope). One of the authors (EMSR) thanks The University of Iowa College of Engineering.

REFERENCES

- Beckermann, C. & Viskanta, R., 1993, Mathematical modeling of transport phenomena during alloy solidification, *Applying Mechanical Review*, vol. 46, n.1, pp. 1-27.
- Bennon, W.D. & Incropera, F.P.A., 1987, Continuum model for momentum, heat and species transport in binary solid-liquid phase change systems - I. Model formulation, *International Journal of Heat and Mass Transfer*, vol. 30, n. 30, pp. 2166-2170.
- El-Bealy, M. & Fredriksson, H., 1991, Effect of thermal strain on macrosegregation in casting processes, *Proceedings of Numerical Methods for Thermal Problems*, International Conference, 8-12 July, Stanford.Irwing, W.R., 1993, *Continuous Casting of Steel*, The Institute of Materials, London.
- Lait, J.E. & Brimacombe, J.K., 1982, Solidification during continuous casting of steel, *ISS Transactions*, vol. 1, pp. 1-13.
- Lesoult, G.; Sella, S., 1990, Analysis and prevention of centerline segregation during continuous casting of steel related to deformation of solid phase, *Proceedings of the Sixth Iron and Steel Congress*, Nagoya, ISIJ, pp. 673-680.
- Maliska, C.R., 1995, *Transferência de Calor e Mecânica dos Fluidos Computacional*. Editora LTC, Rio de Janeiro.
- Miyazawa, K.I. & Schwerdtfeger, K., 1981, Macrosegregation in continuously cast slabs: preliminary theoretical investigation on the effect of steady state bulging, *Arch. Eisenhüttenwes*, vol. 52, n. 11, pp. 415-422.
- Moore, J.J., 1980, Review of axial segregation in continuously cast steel, *Iron and Steelmaker*, vol. 7, n. 10, pp. 8-16.
- Ni, J.; Feller, J.; Beckermann, C., 1991, A two-phase model for transport phenomena during solidification, *Proceedings of Modeling of Casting, Welding and Advanced Solidification Processes V*, TMS, pp. 675-682.
- Nield, D.A. & Bejan, A., 1992, *Convection in Porous Media*, Springer-Verlag, New York.
- Patankar, S.V., 1980, *Numerical Heat transfer and Fluid Flow*, Hemisphere Publishing corporation, Taylor & Francis Group, New York.
- Prescott, P.J. & Incropera, F.P., 1994, Convective transport phenomena and macrosegregation during solidification of a binary metal alloy: I-Numerical predictions, *Journal of Heat Transfer*, vol. 116, pp.735-749.
- Shyy, W.; Udaykumar, H.S.; Rao, M.M.; Smith, R., 1996, *Computational Fluid Dynamics with Moving Boundaries*, Taylor & Francis, Washington.
- Voller, V.R. & Brent, A.D., 1989, The modelling of heat, mass and solute transport in solidification systems, *International Journal of Heat and Mass Transfer*, vol. 32, n. 9 pp. 1719-1731.
- Wang, C.Y. & Beckermann, C., 1993, Single- vs dual-scale volume averaging for heterogeneous multiphase systems, *International Journal of Multiphase Flow*, vol. 19, n. 2, pp. 397-407.
- Zeng, X. & Faghri, A., 1994, Temperature-transforming model for binary solid-liquid phase-change problems part I: mathematical modeling and numerical methodology, *Numerical Heat Transfer B*, pp. 467-479.